Non-Taylor magnetohydrodynamic self-organization

Shao-ping Zhu,[1] Ritoku Horiuchi,[1,2] Tetsuya Sato,[1,2] and Complexity Simulation Group[2,*]
[1]*Department of Fusion Science, The Graduate University for Advanced Studies, Nagoya 464-01, Japan*
[2]*Theory and Computer Simulation Center, National Institute for Fusion Science, Nagoya 464-01, Japan*
(Received 30 September 1994; revised manuscript received 2 February 1995)

A self-organization process in a plasma with a finite pressure is investigated by means of a three-dimensional magnetohydrodynamic simulation. It is demonstrated that a finite pressure, non-Taylor self-organized state is realized in which a perpendicular component of the electric current is generated and a force-free (parallel) current decreases until they reach almost the same level. The self-organized state is described by a magnetohydrodynamic force-balance relation, namely, $\mathbf{j}\times\mathbf{B}=\nabla p$, and the pressure structure resembles the structure of the toroidal magnetic field intensity. The non-Taylor state has a rather universal property, for example, independence of the initial pressure value. Another remarkable finding is that the helicity conservation, in a strict sense, is not satisfied. The magnetic helicity dissipation exhibits a critical slowing down in accordance with the stepwise relaxation of the magnetic energy. It is confirmed that driven magnetic reconnection caused by nonlinearly excited plasma kink flows plays the leading role in all of these key features of the non-Taylor self-organization.

PACS number(s): 52.55.Dy, 52.25.Kn, 52.65.−y, 83.20.Hn

I. INTRODUCTION

In the last two decades, Taylor's theory [1,2] has attracted considerable attention from plasma physicists, because it has been able to predict stable magnetic structures, for example, the field reversal structure of the reversed field pinch (RFP) and the spheromak configuration. Taylor conjectured that a weakly resistive magnetohydrodynamic (MHD) plasma tends to evolve toward a minimum magnetic energy state under the constraint of total magnetic helicity conservation, and predicted that a self-organized state (minimum magnetic energy state) is a force-free equilibrium.

Many numerical simulations [3–10] have attempted to confirm Taylor's conjecture and revealed the dynamical behavior of the self-organization process. Through a three-dimensional full MHD simulation study Horiuchi and Sato [6,7] demonstrated that the nonlinear driven magnetic reconnection plays a key role in the self-organization process of a MHD plasma. For instance, through the nonlinear driven magnetic reconnection process the spectrum of magnetic energy exhibits a normal cascade while that of magnetic helicity shows an inverse cascade. The phenomenon that the dissipation rate of magnetic energy is faster than the dissipation rate of magnetic helicity is also explained in terms of the driven magnetic reconnection.

It should be emphasized here that Taylor's theory can only be applied to a case where the plasma pressure is uniform throughout the whole system. In reality, however, an excess free magnetic energy is transformed into thermal energy. In general, the released thermal pressure has a spatial structure because of the spatial dependence of the current density or resistivity. Though in plasmas there are a few mechanisms that lead to redistribution of thermal energy, i.e., convection, expansion, thermal conduction, and so on, it is not a natural consequence that the plasma pressure becomes homogeneous. Many efforts have been made to extend Taylor's theory to a finite pressure MHD plasma [8–12]. However, most of the works have reached Taylor's force-free state. Recently, Kondoh *et al.* [13] have dealt with this problem from a different viewpoint and asserted that the self-organized state becomes a non-force-free one if the electrical resistivity has a spatial dependence. For spatially uniform electrical resistivity, however, their state also degenerated into the Taylor state.

In order to bring out clearly the effect of the plasma pressure on the self-organization process of a MHD plasma, we employ a three-dimensional MHD simulation code [14] with a fourth-order accuracy in both time and space in this paper.

The plan of the paper is as follows. In Sec. II we explain our simulation model. The simulation results are presented in Sec. III. Section IV contains a brief summary of the present study.

II. SIMULATION MODEL

We consider a compressible, dissipative MHD plasma with a finite pressure confined in a conducting cylindrical vessel with a rectangular cross section. The basic equations are described in dimensionless form as

$$\frac{\partial\rho}{\partial t}=-\nabla\cdot(\rho\mathbf{v})\ , \tag{1}$$

$$\frac{\partial\mathbf{F}}{\partial t}=-\nabla\cdot(\mathbf{F}\mathbf{v})-\nabla p+\mathbf{j}\times\mathbf{B}\ , \tag{2}$$

$$\frac{\partial\mathbf{B}}{\partial t}=\nabla\times(\mathbf{v}\times\mathbf{B}-\eta\mathbf{j})\ , \tag{3}$$

*K. Watanabe, T. Hayashi, Y. Todo, T. H. Watanabe, A. Kageyama, and H. Takamaru.

$$\frac{\partial p}{\partial t} = -\nabla\cdot(p\mathbf{v}) + (\gamma-1)(-p\nabla\cdot\mathbf{v} + \eta\mathbf{j}\cdot\mathbf{j}) , \quad (4)$$

where

$$\mathbf{j} = \nabla\times\mathbf{B} , \quad (5)$$

and $\mathbf{F}$ $(=\rho\mathbf{v})$ is the mass flux density, p is the thermal pressure, ρ is the mass density, $\mathbf{v}$ is the fluid velocity, $\mathbf{B}$ is the magnetic field, $\mathbf{j}$ is the current density, η is the uniform electrical resistivity, and γ $(=\frac{5}{3})$ is the ratio of the specific heats. In general, the thermal conduction term should be added in Eq. (4). Since we are primarily interested in the structure of the plasma pressure in this paper, we focus our attention on the case where the effect of thermal conduction is discarded and the vessel is thermally insulated.

In order to accomplish our motivation of elucidating the physical influence of the thermal energy converted from the magnetic energy on MHD self-organization, it is required that the numerical diffusion of pressure be sufficiently small not to smear out the generated pressure structure during the relaxation process of concern. To fulfill this requirement, we employ a high-precision simulation code [14] which is based on an explicit finite-difference method with fourth-order accuracy in both space and time. The simulation domain is implemented on a $100\times100\times150$ point grid. By this choice it becomes possible to disclose rather fine structures of pressure, which were missed in the previous work based on the two-step Lax-Wendroff scheme [8].

A Cartesian coordinate system (x,y,z) is employed. The system is periodic along the z axis with a periodic length L_t, and is surrounded by a conducting wall at $x=0$ and L_p, and $y=0$ and L_p, i.e., $\mathbf{n}\cdot\mathbf{v}=0$, $\mathbf{n}\times\mathbf{j}=\mathbf{0}$, and $\mathbf{n}\cdot\mathbf{B}=0$, where $\mathbf{n}$ is the unit vector normal to the conducting surface. As an initial condition we impose a two-dimensional force-free equilibrium [7] in which the pressure and the mass density have uniform spatial profiles. The initial magnetic configuration is shown in Fig. 1 where the right and left panels correspond to the vector plots of the poloidal magnetic field and the contour plots of the toroidal magnetic field intensity in the poloidal plane (x,y), respectively.

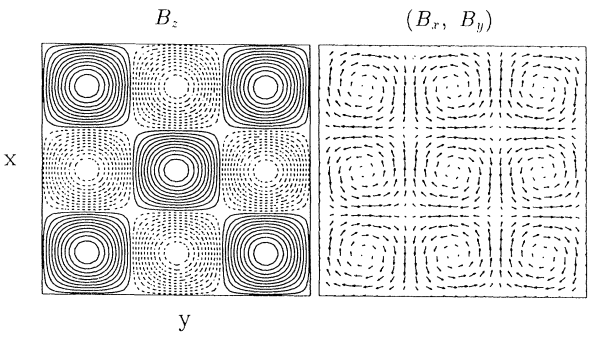

FIG. 1. The vector plots of the poloidal magnetic field (right) and the contour plots of the toroidal magnetic field (left) in a poloidal plane (x,y) at $t=0$ where a contour with a negative toroidal field is plotted by a dotted line.

There are three important parameters to characterize the energy relaxation process of a MHD plasma, i.e., (a) the initial normalized magnetic helicity α $(=2\pi L_p K/L_t\psi^2)$, (b) the initial normalized magnetic energy ϵ $(=L_p W/2K)$, and (c) the ratio of the side lengths L_t/L_p, where K and W are the total magnetic helicity and energy, respectively, and ψ $(=\int B_z dx\,dy)$ is the total toroidal magnetic flux. In this paper, we assume $\alpha=58.3$, $\epsilon=6.7$, and $L_t/L_p=3$. Taylor's relaxation theory [1,7,15] predicts that our system relaxes to a helically symmetric state with the toroidal mode number of $n=1$.

III. SIMULATION RESULTS

Five simulation runs with different initial values of the plasma β and the resistivity η are carried out where the values of β and η are listed in Table I. In the following discussion, we analyze the simulation result for case A given in Table I unless otherwise stated.

A. Fundamental properties of energy relaxation

Previous papers [6–9] have revealed two important characteristics of the MHD self-organization, namely, (1) slow decay of magnetic helicity and selective dissipation of magnetic energy, and (2) normal cascade of the magnetic energy spectrum and inverse cascade of the magnetic helicity spectrum. Figure 2 shows, with the high-precision simulation code, the temporal evolutions of the total magnetic energy W (dashed line) and the total magnetic helicity K (solid line) where W and K are normalized by their initial values and the time is normalized by the Alfvén transit time t_A. The behavior of the magnetic energy W illustrates that there appear two relaxation phases in the temporal evolution, i.e., the first relaxation phase $(18t_A < t < 25t_A)$ and the second relaxation phase $(35t_A < t < 46t_A)$. The magnetic energy dissipates rapidly in the relaxation phases in the time scale comparable to the Alfvén transit time. In contrast to the stepwise relaxation of magnetic energy, the rate of magnetic helicity exhibits explicitly a stepwise slowing down in accordance with the stepwise drop of magnetic energy. This critical slowing down phenomenon has never been proposed theoretically [1,2,11–13] nor discovered numerically [3–9].

We now investigate how and why selective dissipation of magnetic energy and critical slowing down of the dissipation rate of magnetic helicity occur. From the MHD equations (1)–(4), the total magnetic energy and the total magnetic helicity decrease according to the following relations:

TABLE I. Simulation parameters.

Case	α	β	η
A	58.3	0.6	10^{-4}
B	58.3	0.6	2×10^{-4}
C	58.3	0.6	5×10^{-4}
D	58.3	0.4	2×10^{-4}
E	58.3	0.2	2×10^{-4}

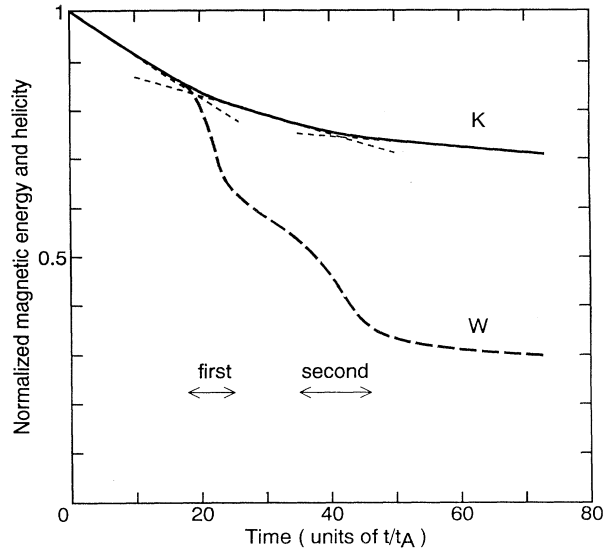

FIG. 2. The temporal evolutions of the total magnetic energy W (dashed line) and the total magnetic helicity K (solid line) for case A where both the energy and the helicity are normalized by their initial values.

$$\frac{dW}{dt} \simeq -\eta \int \mathbf{j}\cdot\mathbf{j}\, d^3\mathbf{x} , \tag{6}$$

and

$$\frac{dK}{dt} = -\eta \int \mathbf{j}\cdot\mathbf{B}\, d^3\mathbf{x} . \tag{7}$$

These relations imply that, if the force-free relation $\mathbf{j}=\mu\mathbf{B}$ holds, both magnetic energy and magnetic helicity dissipate in a similar fashion. We plot in Fig. 3(a) the temporal evolutions of the total energy dissipation D_W and the total helicity dissipation D_K where $D_W=\int(\mathbf{j}\cdot\mathbf{j})d^3\mathbf{x}$ and $D_K=\int(\mathbf{j}\cdot\mathbf{B})d^3\mathbf{x}$. In the initial phase ($0<t<18t_A$) these quantities decrease with the same rate. This means that the force-free relaxation approximately holds in this period. However, one sees that the energy dissipation rate increases drastically as soon as the first and second relaxations set in, and its value becomes much larger than that expected from the force-free state. In contrast, the rate of helicity dissipation exhibits explicitly a slowing down at each relaxation phase of the magnetic energy. In order to see directly why energy dissipation is enhanced and helicity dissipation is reduced, we plot in Fig. 3(b) the bird's-eye views of the spatial profiles of $\mathbf{j}\cdot\mathbf{j}$ (top) and the negative component of $\mathbf{j}\cdot\mathbf{B}$ (bottom) in the poloidal cross section ($z=L_z/2$) at the time $t=20.43t_A$. One can explicitly see that the value of $\mathbf{j}\cdot\mathbf{j}$ is sharply peaked in the vicinity of the reconnection points caused by kink flows, while that of $\mathbf{j}\cdot\mathbf{B}$ is negatively peaked at the same reconnection regions. (Note here that $\mathbf{j}\cdot\mathbf{B}>0$ everywhere in the initial state.) The sharp peakings of $\mathbf{j}\cdot\mathbf{j}$ and $-\mathbf{j}\cdot\mathbf{B}$ at the reconnection points act to anomalously enhance the dissipation rate of magnetic energy and to critically reduce the dissipation rate of magnetic helicity. This is due to the fact that the reconnection current is now reversed, i.e., opposite to the initial current. Since the production of such enhanced current peaks is brought about by kink flows, we can conclude that the driven reconnection process is the key to MHD self-organization.

Next we shall proceed to the identification of modes that contribute to driven reconnections of the first and second relaxations. The temporal evolutions of two Fourier modes of the y component of the magnetic field

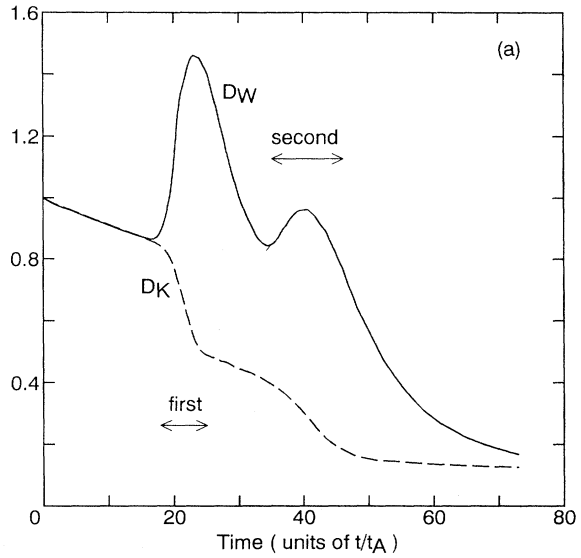

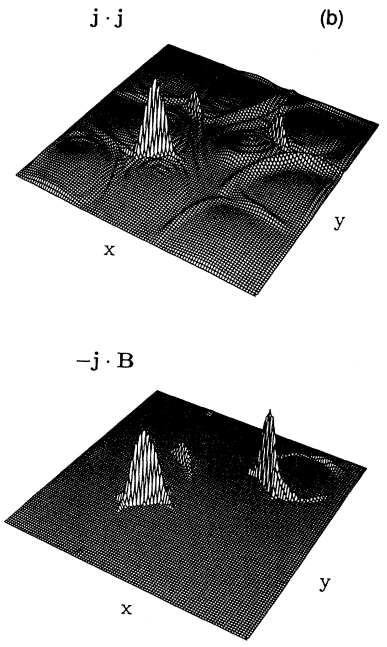

FIG. 3. (a) The temporal evolutions of the total energy dissipation D_W and the total helicity dissipation D_K in the same case as Fig. 2, where $D_W=\int(\mathbf{j}\cdot\mathbf{j})d^3\mathbf{x}$ and $D_K=\int(\mathbf{j}\cdot\mathbf{B})d^3\mathbf{x}$. (b) The bird's-eye views of the profiles for $\mathbf{j}\cdot\mathbf{j}$ (top) and $-\mathbf{j}\cdot\mathbf{B}$ (bottom) in the poloidal cross section ($z=L_z/2$) at $t=20.43t_A$ for case A, where only the negative part of $\mathbf{j}\cdot\mathbf{B}$ is displayed in the bottom panel.

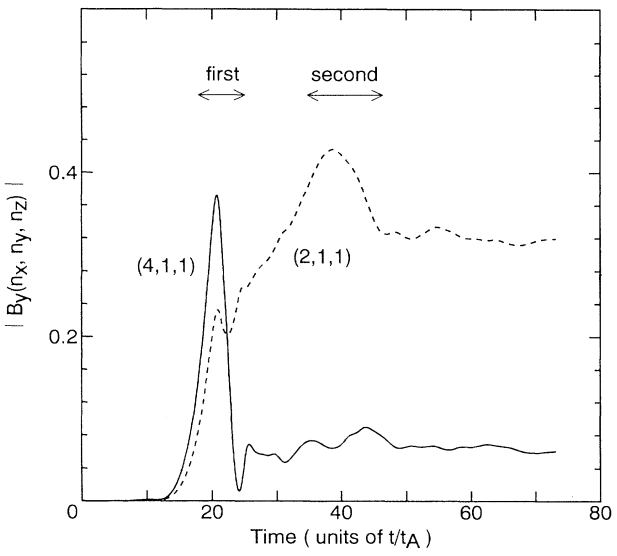

FIG. 4. The temporal evolution of two Fourier modes of the y component of the magnetic field B_y in the same case as Fig. 2. The amplitudes are normalized by the initial value of B_y.

B_y are shown in Fig. 4. From this figure, one can confirm that the first relaxation phase is caused by the helical kink mode $(n_x,n_y,n_z)=(4,1,1)$, while the second relaxation phase is caused by the excitation of a different mode, namely, the mode $(n_x,n_y,n_z)=(2,1,1)$.

B. Finite β self-organization

We now study the self-organized structure in a finite pressure MHD plasma. Figure 5 shows the contour maps of the toroidal magnetic field (top) and the pressure (bottom) at $t=19.0t_A$ (left), $t=32.4t_A$ (middle), and $t=71.3t_A$ (right) for $\beta=0.6$ and $\eta=5\times10^{-4}$ (case C) where the red color stands for a contour larger than the average value of the pressure (lower part) and a positive toroidal magnetic field (upper part). It is evident that a clear structure of pressure is developed along the new magnetic structure, and that the two profiles are similar.

There are two processes that lead to an increase in the thermal pressure; the first one is the slow heating process which is governed by the resistive diffusion process prior to the onset of the first reconnection, and the other one is the fast heating process which is associated with driven magnetic reconnection. In the early phase $(0<t<18t_A)$,

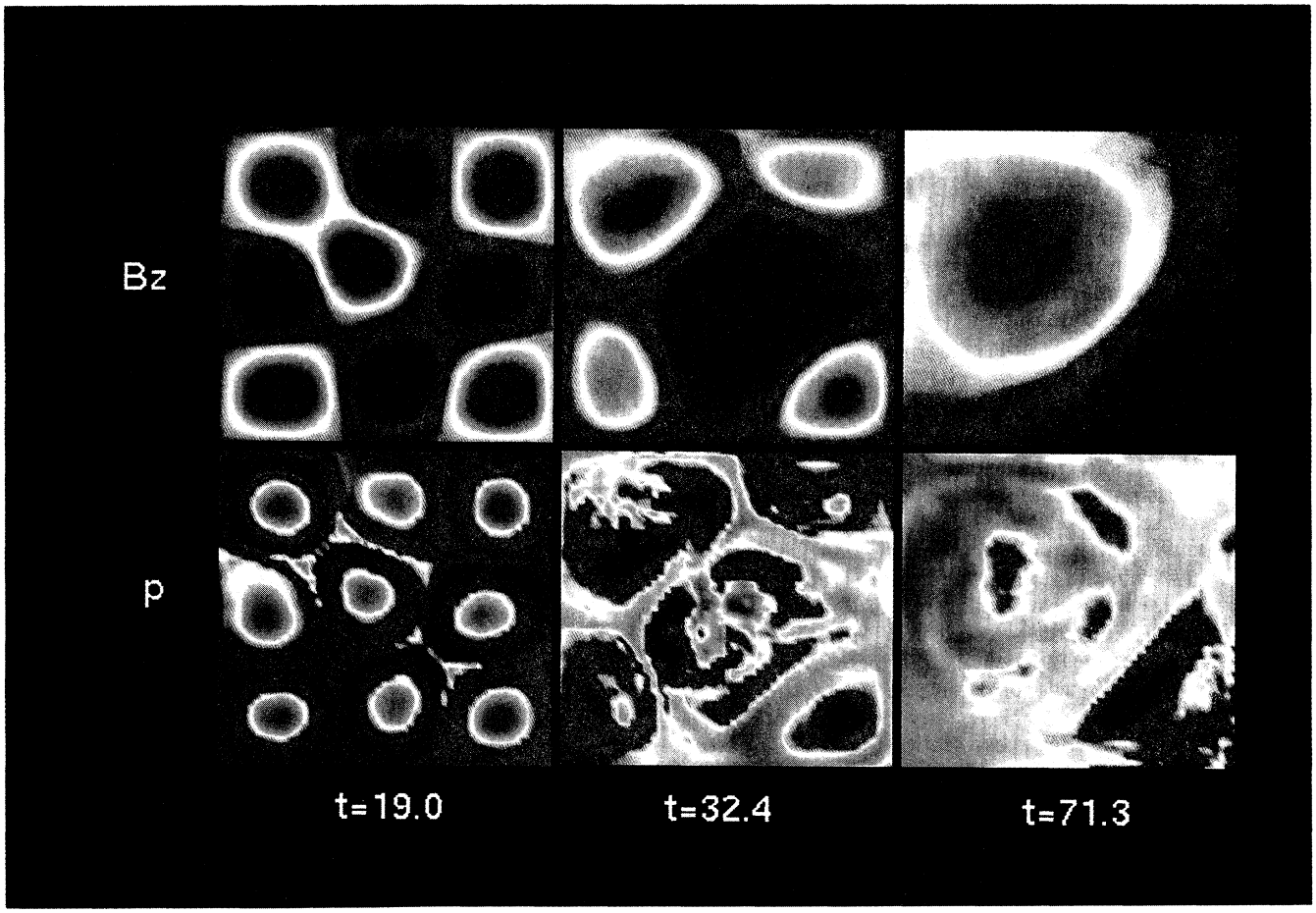

FIG. 5. The contour maps of the toroidal magnetic field (top) and the pressure (bottom) at $t=19.0t_A$ (left), $t=32.4t_A$ (middle), and $t=71.3t_A$ (right) for case C where the red color stands for a contour larger than the average value of p or the positive toroidal magnetic field.

the magnetic field intensity decreases diffusively in the resistive time scale and approximately keeps the same spatial pattern as the initial magnetic field pattern and hence the initial electric current pattern. Therefore the spatial structure of the pressure created through Ohmic heating becomes similar to that of the initial current pattern, equivalent to that of the magnetic field pattern (left panels). This heating process is the slow one in which the amount of enhanced heat is proportionally dependent on the value of the electrical resistivity.

Nonlinear magnetic reconnection is driven as a result of the strong development of an ideal kink instability. Driven reconnection combines the four original negative magnetic flux tubes into one big tube in the central part and the five original positive tubes into four tubes on the four corners in the first relaxation phase (upper middle panel in Fig. 5). This process is the fast one in which rapid transfer of magnetic energy to thermal energy arises. Since reconnection takes place at a local minimum point of the original force-free current, the pressure profile generated by this driven magnetic reconnection process is peaked at the local minimum point of the pressure profile generated by the early slow process. The enhanced pressure-gradient force (slow shock) generates fast outflows whereby the thermal energy and the reconnected magnetic flux are carried away along the field line from the reconnection point; thus the pressure structure is aligned along the field line.

Thereafter, the second relaxation takes place and the four positive flux tubes are merged into one flux tube through the driven magnetic reconnection process. The pressure maintains a clear structure similar to the magnetic structure even in the final stage.

Since the kink and reconnection flows transverse to the field lines are relatively small and decay after the second relaxation, the localized structure of thermal pressure obtained is sustained for a fairly long time. Figure 6 shows the temporal evolution of the pressure deviation δp from the average defined by

$$\delta p = \left\{ \frac{\langle (p - \langle p \rangle)^2 \rangle}{\langle p \rangle^2} \right\}^{1/2} \tag{8}$$

for three different resistivities, namely cases A (solid line), B (dashed line), and C (dot-dashed line) given in Table I, where $\langle f(\mathbf{x}) \rangle$ stands for the average of $f(\mathbf{x})$ over the whole volume. The pressure deviation increases slowly and proportionally to the resistivity in the early quiet Ohmic diffusion phase as is expected. As soon as the first relaxation sets in it suddenly shoots up. Its time scale is a few times the Alfvén transit time. It is important to note that the pressure deviation in the fast relaxation phase becomes more enhanced as the resistivity decreases, in contrast to the fact that the pressure deviation is more reduced as the resistivity decreases in the slow diffusion process.

In driven reconnection [16–19] the reconnection current $j_{\rm rec}$ is roughly given by equating the reconnection electric field $\eta j_{\rm rec}$ to the driving electric field E_d, which is given by the flow velocity of an unstable ideal kink mode. The transfer rate of magnetic energy into thermal energy

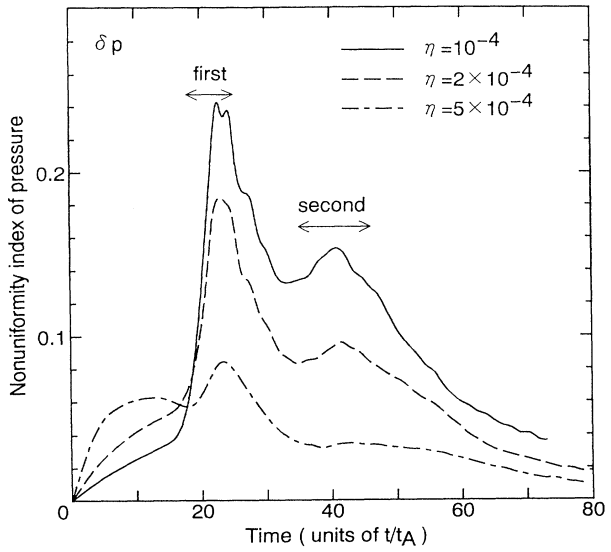

FIG. 6. The temporal evolutions of the average pressure fluctuation δp for case A (solid line), case B (dashed line), and case C (dot-dashed line).

$\eta j_{\rm rec}^2$ is given as E_d^2/η [16–19]. Since the flow velocity of an ideal kink mode is independent of η, the energy transfer rate of the fast process decreases with resistivity. Thus the remarkable features seen in Fig. 6 are consistent with the driven reconnection process.

We shall next examine the state of the system after the second relaxation. We decompose the electric current into the force-free (parallel) component and the perpendicular component and plot their temporal evolutions in Fig. 7 for cases A (solid line), B (dashed line), and C (dot-dashed line), where $J_\parallel = \langle |\mathbf{j}_\parallel|/|\mathbf{j}| \rangle$, $J_\perp = \langle |\mathbf{j}_\perp|/|\mathbf{j}| \rangle$, $\mathbf{j}_\parallel = (\mathbf{j}\cdot\mathbf{B})\mathbf{B}/(\mathbf{B}\cdot\mathbf{B})$, and $\mathbf{j}_\perp = \mathbf{j} - \mathbf{j}_\parallel$. From this figure one

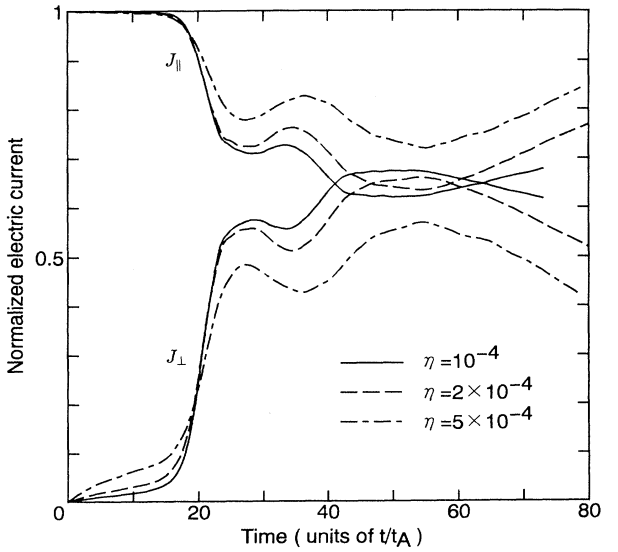

FIG. 7. The temporal evolutions of the normalized parallel component $J_\parallel$ and the normalized perpendicular component $J_\perp$ of the electric current for the same cases as Fig. 6, where $J_\parallel = \langle |\mathbf{j}_\parallel|/|\mathbf{j}| \rangle$ and $J_\perp = \langle |\mathbf{j}_\perp|/|\mathbf{j}| \rangle$.

can evidently see that the perpendicular component increases rapidly in accordance with the growth of the ideal kink instability in the first relaxation phase. It increases again in the second relaxation phase and reaches a value comparable to the parallel component. The amplitude attained is roughly maintained until the end of the simulation run. Consequently, we can conclude that the system relaxes to an equilibrium state and this state is absolutely different from Taylor's force-free minimum energy state where $J_\perp$ vanishes.

C. Non-Taylor relaxation

We are now in a position to elucidate the structure which is realized in a MHD plasma in the presence of thermal pressure and the nature of which is different from what is predicted by Taylor's conjecture for the pressureless case. Figure 8 shows a three-dimensional display of the isosurfaces of the toroidal magnetic field (left) and the thermal pressure (right) at $t=0$, $t=19.0t_A$, $t=32.4t_A$, and $t=71.3t_A$ for case *C*, where the yellow and red isosurfaces stand for the positive value and the negative value, respectively. There exist five positive flux tubes and four negative flux tubes at $t=0$. This spatial structure is deformed into an intermediate one with one negative helical flux tube and four positive flux tubes through the driven magnetic reconnection process in the first relaxation phase. Finally, the system self-organizes into a helically symmetric state of the toroidal mode number $n=1$ in which one positive helical flux tube and one negative flux tube exist. At a glance, this simulation result appears similar to the self-organized state expected from the relaxation theory for the pressureless plasma [15]. As mentioned above, however, the spatial structure of the thermal pressure is not uniform even at the final stage and hence the final equilibrium state is considered to be different from the force-free one.

In order to identify what kind of state is achieved at the final state of the present simulation, we have exam-

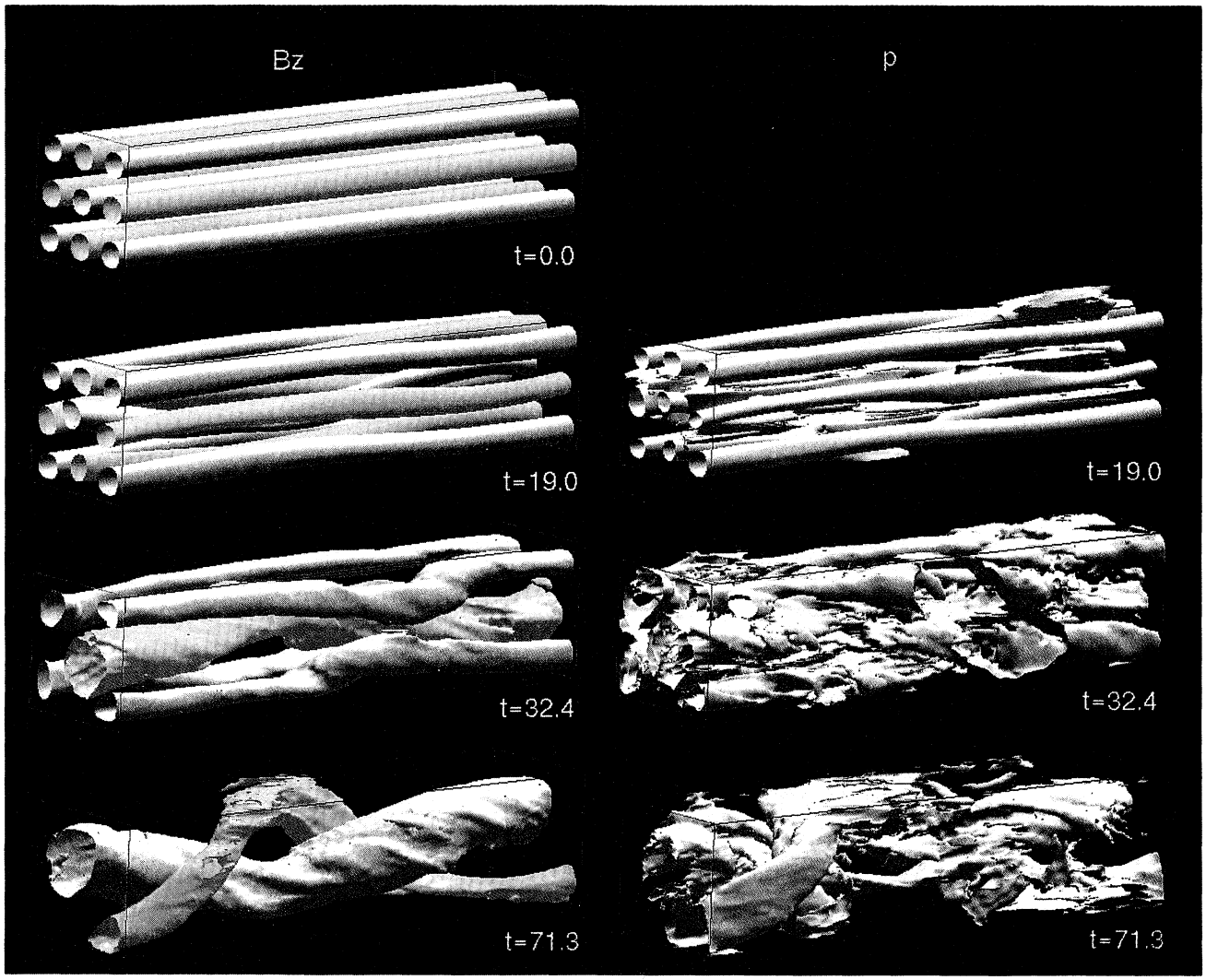

FIG. 8. A three-dimensional display of the isosurfaces of the toroidal magnetic field and the pressure at $t=0$, $t=19.0t_A$, $t=32.4t_A$, and $t=71.3t_A$ for case *C*.

ined the spatial structures of the pressure gradient and $\mathbf{j}\times\mathbf{B}$ force and confirmed that the achieved state is almost a force-balanced equilibrium where $\mathbf{j}\times\mathbf{B}=\nabla p$ is satisfied at every point in the system.

Figure 9 shows the temporal evolution of the total kinetic energy. This figure clearly indicates that the kinetic energy increases in good coincidence with the first and second relaxation phases and vanishes toward the end of the simulation run. This feature, along with the existence of a sizable pressure gradient, gives another evidence that the self-organized state is a force-balanced equilibrium.

D. Independence of the initial plasma β

The existence of a finite thermal pressure makes the relaxed state different from Taylor's force-free one. We have examine the dependence of the deviation from the Taylor structure on the initial β value. Figure 10(a) shows the temporal evolutions of the parallel component $J_{\parallel}$ and the perpendicular component $J_{\perp}$ of the electric current for three cases with different initial β given in Table I, namely, for case B ($\beta=0.6$), case D ($\beta=0.4$), and case E ($\beta=0.2$). As a whole, no significant difference is observed among the three cases except that the onset time of the relaxation phase is slightly delayed as β increases. The perpendicular component, which is generated during the two relaxation phases, remains finite even in the final equilibrium state and the amplitude is comparable to that of the parallel component regardless of the value of β for $\beta=0.2$–0.6. Figure 10(b) shows the temporal evolution of the time scale function $R(t)$ for the same cases as Fig. 10(a). $R(t)$ is the ratio of the time scale for the magnetic helicity dissipation τ_{MH} to the time scale for the magnetic energy dissipation τ_{ME}, where $R(t)$, τ_{ME}, and τ_{MH} are defined by

$$R(T)=\frac{\tau_{\mathrm{MH}}}{\tau_{\mathrm{ME}}}\,, \tag{9}$$

$$\tau_{\mathrm{ME}}=\frac{\int \mathbf{B}\cdot\mathbf{B}\,d^3\mathbf{x}}{2\eta\int \mathbf{j}\cdot\mathbf{j}\,d^3\mathbf{x}}\,, \tag{10}$$

$$\tau_{\mathrm{MH}}=\frac{\int \mathbf{A}\cdot\mathbf{B}\,d^3x}{2\eta\int \mathbf{j}\cdot\mathbf{B}\,d^3\mathbf{x}}\,. \tag{11}$$

One can see that all the results are essentially superimposable with the exception of a slight delay in the onset

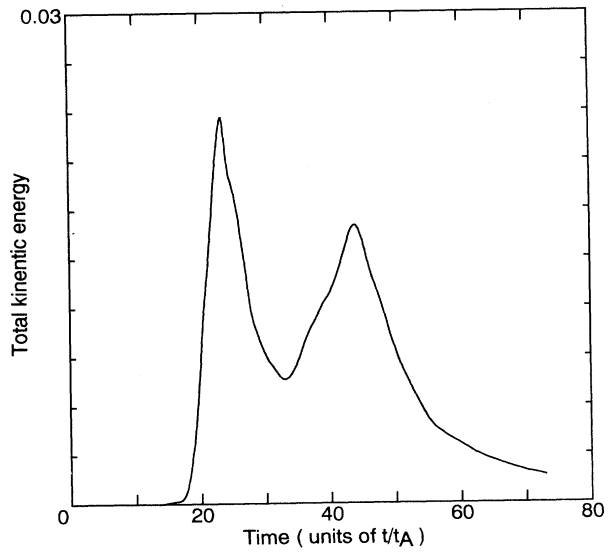

FIG. 9. The temporal evolution of total kinetic energy for case A.

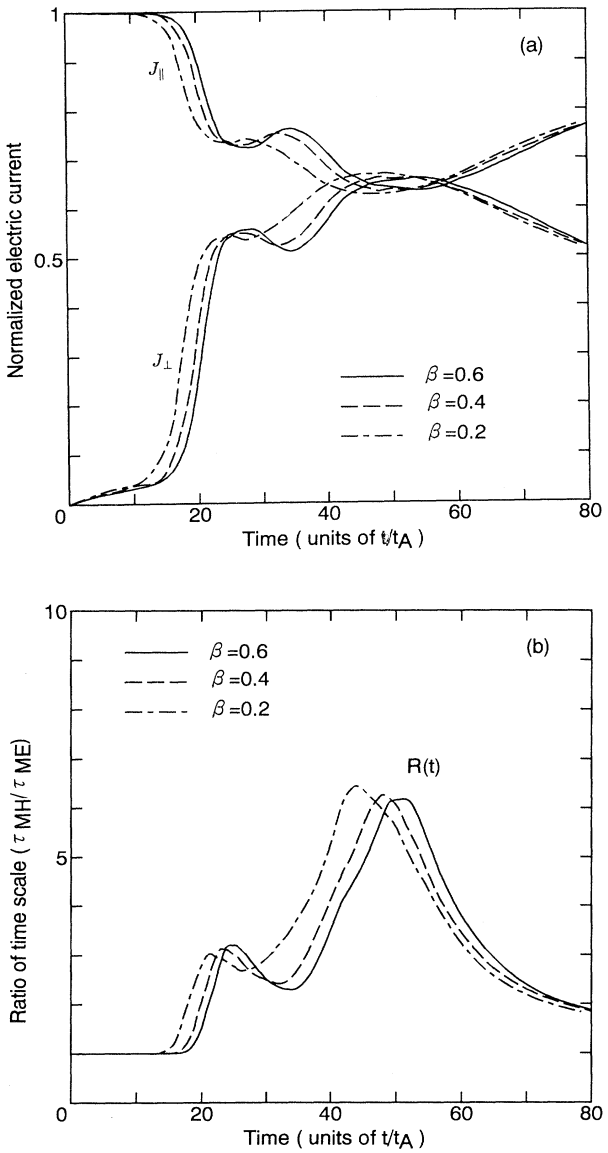

FIG. 10. (a) The temporal evolutions of the normalized parallel component $J_{\parallel}$ and the normalized perpendicular component $J_{\perp}$ of the electric current for case B ($\beta=0.6$), case D ($\beta=0.4$), and case E ($\beta=0.2$), respectively. (b) The temporal evolutions of the function $R(t)$, where $R(t)$ is the ratio of the time scale for the magnetic helicity dissipation to the time scale for the magnetic energy dissipation.

times of the first and second relaxation phases for a high initial β plasma. Thus it is concluded that both the plasma behavior in the relaxation phase and the final relaxed state are almost independent of the initial amount of thermal pressure. This conclusion can be understood as follows. There are two physical processes that make the pressure uniform. One is expansion and the other is convection. For the case with finite pressure, both of them are very weak compared with the fast heating process. Consequently, we can conclude that in the absence of some rapid process which pumps out the produced thermal energy the system will experience a non-Taylor (non-force-free) self-organization.

IV. SUMMARY

With a three-dimensional simulation study we have investigated the self-organization process of a finite pressure MHD plasma under the condition that the plasma is thermally insulated perpendicular to the magnetic field. It is confirmed that driven magnetic reconnection plays a crucial role in the self-organization process. It is driven magnetic reconnection that actuates the selective dissipation of magnetic energy. The present elaborate study has revealed that during the two-step relaxation process subject to driven reconnection the decay rate of magnetic helicity is critically slowed down. This implies that helicity conservation is not a substantiated property for MHD self-organization, though this has been widely believed so far.

It is also found that the onset time of driven magnetic reconnection is almost independent of the electrical resistivity. For a case with an exceptionally large electrical resistivity, the magnetic reconnection process becomes not so conspicuous because most of the free magnetic energy dissipates before the first magnetic reconnection takes place and the process becomes almost diffusive. This indicates that a "weak electrical resistivity" condition, or a collisionless condition, is necessary for a clear-cut self-organization to take place.

We have demonstrated that a finite pressure MHD plasma system relaxes toward a state with a minimum magnetic energy which is similar to the pressureless case. This is because the most important physical process in self-organization is the driven magnetic reconnection process and the pressure is not the primary cause of reconnection. However, the magnetic field configuration is not described by Taylor's force-free minimum energy state. The driven magnetic reconnection process produces an extremely heated plasma in the vicinity of a reconnection point. The locally heated plasma modifies the magnetic field. As a result of the produced pressure gradient, the perpendicular electric current is generated to balance the pressure gradient force. It is confirmed that the new self-organized state of a finite pressure MHD plasma is a MHD equilibrium $\mathbf{j}\times\mathbf{B}=\nabla p$, instead of Taylor's minimum energy state. We have also confirmed that there is no significant effect of the initial plasma β on this conclusion. This suggests that, as long as the thermal energy produced by the relaxation process is confined within a system where neither fast thermal conduction nor radiation cooling exist, the MHD plasma does not obey the Taylor relaxation process, but experiences a non-Taylor process which leads to a force-balanced minimum energy state.

ACKNOWLEDGMENTS

This work was performed by using the Advanced Computing System for Complexity Simulation at NIFS under the support of two Grants-in-Aid from the Japanese Ministry of Education, Science and Culture (No. 05836038 and No. 06044238). One of the authors (S.P.Z.) would like to thank Professor X. T. He for his support. S.P.Z. is supported by the Japanese Ministry of Education, Science and Culture (MONBUSHO).

[1] J. B. Taylor, Phys. Rev. Lett. **33**, 1139 (1974).
[2] J. B. Taylor, Rev. Mod. Phys. **58**, 741 (1986), and references therein.
[3] W. H. Matthaeus and D. C. Montgomery, Ann. N.Y. Acad. Sci. **357**, 203 (1980).
[4] W. H. Matthaeus, M. L. Goldstein, and D. C. Montgomery, Phys. Rev. Lett. **51**, 1484 (1983).
[5] A. Y. Aydemir and D. C. Barnes, Phys. Rev. Lett. **52**, 930 (1984).
[6] R. Horiuchi and T. Sato, Phys. Rev. Lett. **55**, 211 (1985).
[7] R. Horiuchi and T. Sato, Phys. Fluids **29**, 1161 (1986).
[8] R. Horiuchi and T. Sato, Phys. Fluids **29**, 4174 (1986).
[9] R. Horiuchi and T. Sato, Phys. Fluids **33**, 1142 (1988).
[10] S. Ortolani and D. D. Schnack, *Magnetohydrodynamics of Plasma Relaxation* (World Scientific, Singapore, 1993).
[11] A. Bhattacharjee and R. L. Dewar, Phys. Fluids **25**, 887 (1982).
[12] J. W. Edenstrasser and W. Schuurman, Phys. Fluids **26**, 500 (1983).
[13] Y. Kondoh, Y. Hosaka, J. L. Liang, R. Horiuchi, and T. Sato, J. Phys. Soc. Jpn. **63**, 546 (1994).
[14] R. Horiuchi and T. Sato, Phys. Fluids B **1**, 581 (1989).
[15] A. Reiman, Phys. Fluids **23**, 230 (1980).
[16] T. Sato and T. Hayashi, Phys. Fluids **22**, 1189 (1979).
[17] T. Sato, T. Hayashi, K. Watanabe, R. Horiuchi, M. Tanaka, N. Sawairi, and K. Kusano, Phys. Fluids B **4**, 450 (1992).
[18] T. Sato and K. Kusano, Phys. Rev. Lett. **54**, 808 (1985).
[19] T. Sato, R. Horiuchi, and K. Kusano, Phys. Fluids B **1**, 225 (1989).

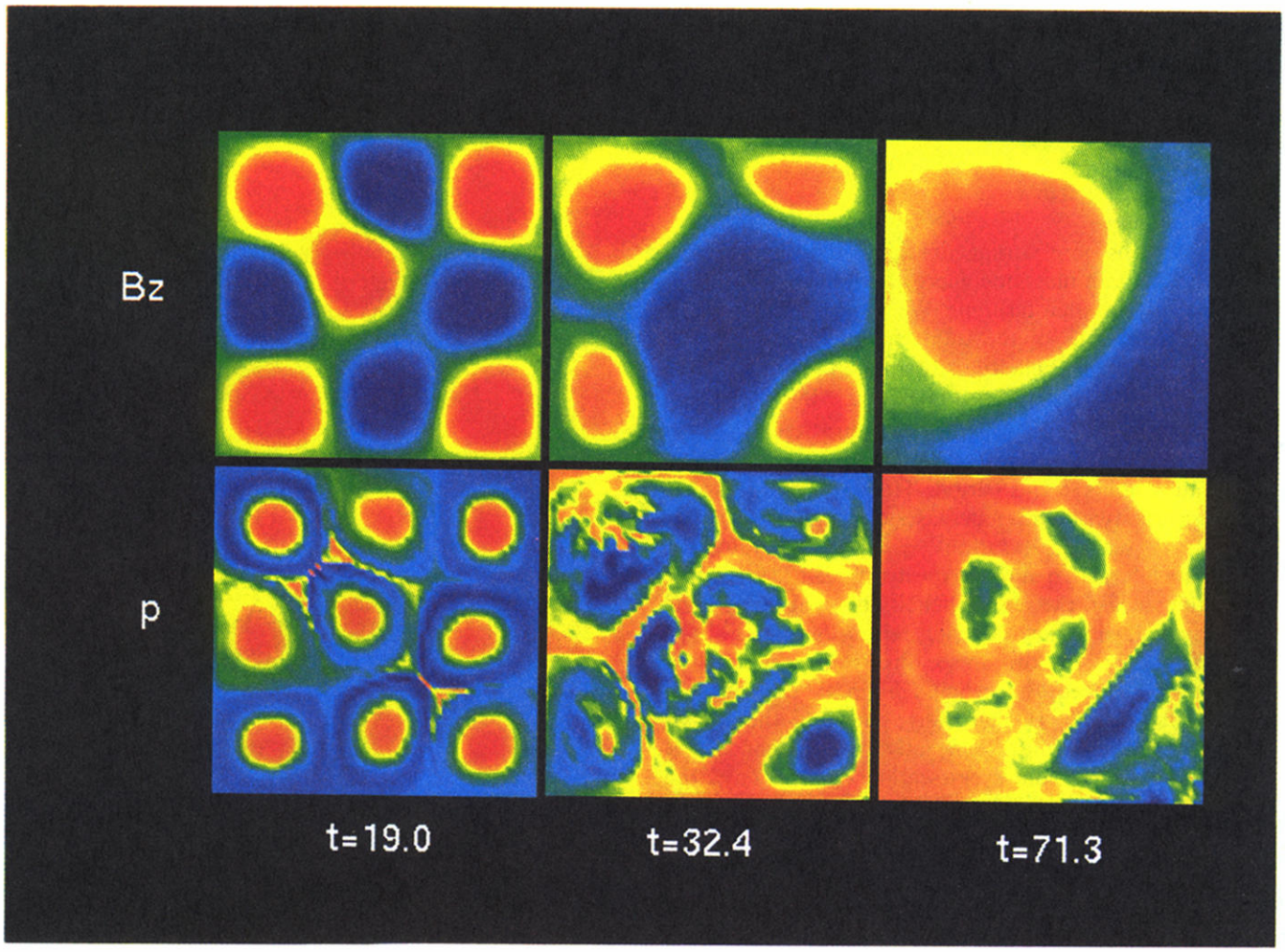

FIG. 5. The contour maps of the toroidal magnetic field (top) and the pressure (bottom) at $t = 19.0t_A$ (left), $t = 32.4t_A$ (middle), and $t = 71.3t_A$ (right) for case C where the red color stands for a contour larger than the average value of p or the positive toroidal magnetic field.

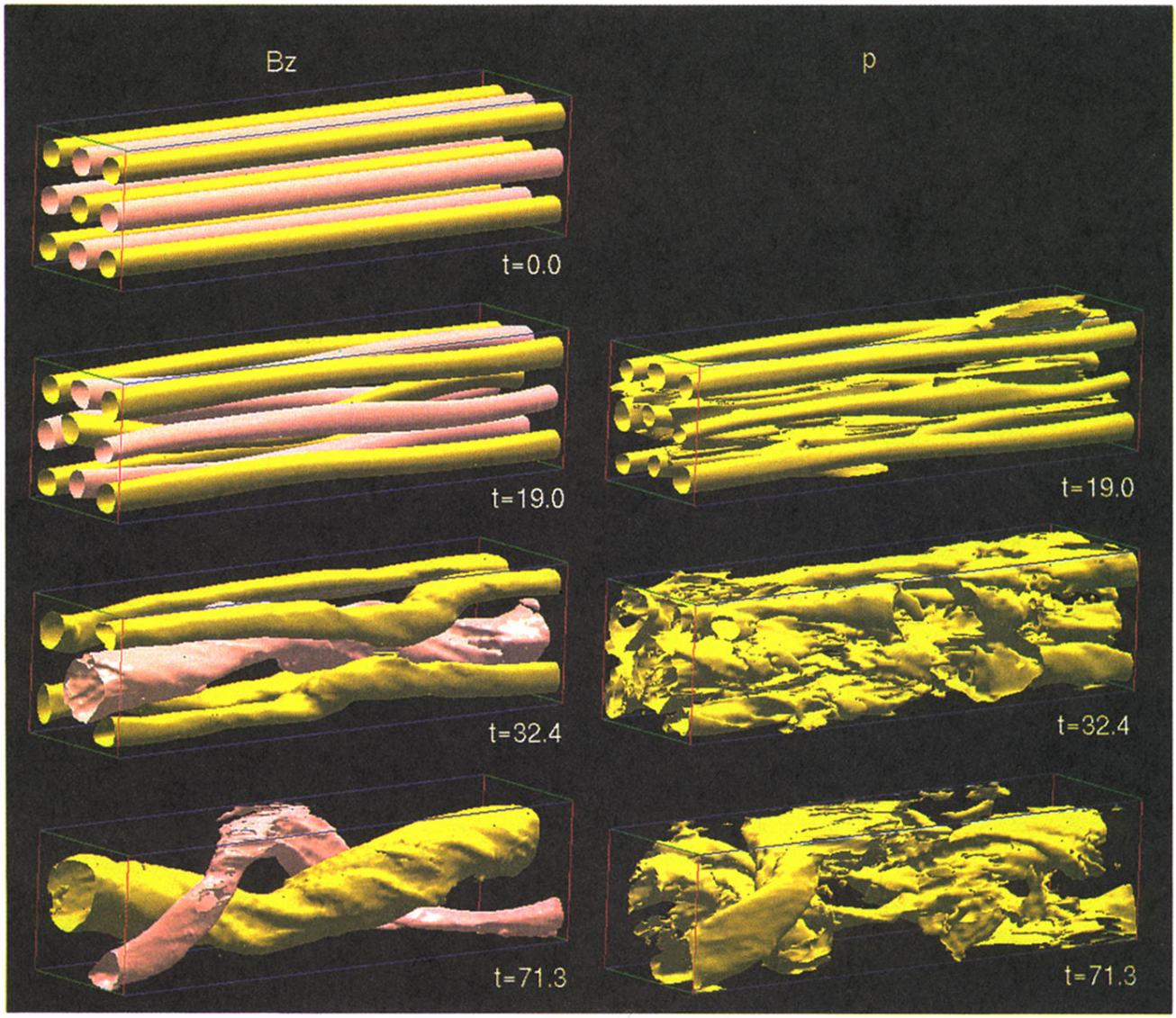

FIG. 8. A three-dimensional display of the isosurfaces of the toroidal magnetic field and the pressure at $t=0$, $t=19.0t_A$, $t=32.4t_A$, and $t=71.3t_A$ for case *C*.